Journal of Fluorine Chemistry 132 (2011) 907–914

Contents lists available at ScienceDirect

Journal of Fluorine Chemistry

journal homepage: www.elsevier.com/locate/fluor

Theoretical study of thiazole derivatives as chemosensors for fluoride anion

Ruifa Jin *

College of Chemistry and Chemical Engineering, Chifeng University, Chifeng 024000, China

ARTICLE INFO

Article history:
Received 22 April 2011
Received in revised form 1 July 2011
Accepted 6 July 2011
Available online 12 July 2011

Keywords:
2-(2′-Hydroxyphenyl)-4-phenylthiazole
Chemosensor
BSSE (counterpoise) correction
Intramolecular charge transfer (ICT)
Atoms in molecules (AIM)

ABSTRACT

The interactions between chemosensor, 2-(2′-hydroxyphenyl)-4-phenylthiazole (**1**), and different halides (F^-, Cl^-, and Br^-) and NO_3^- anions have been theoretically investigated at the B3LYP/6-31G(d) level with the BSSE correction. It turned out that the unique selectivity of **1** for F^- is ascribed to its ability of deprotonating the hydroxy group of host sensor. The intermolecular proton transfer (IPT) causes the colorimetric and fluorescent signaling of **1** for F^-. The deprotonated complex $\mathbf{1}^-$·HF is formed for the deprotonation process of chemosensor. The study of substituent effects suggest that the electron-donating $-CH_3$ and $-OCH_3$ substituted derivatives are expected to be promising candidates for ratiometric fluorescent F^- chemosensors as well as chromogenic chemosensors, while electron-donating $-N(CH_3)_2$ substituted derivative can serve as chromogenic F^- chemosensors only. Furthermore, the electron-withdrawing ($-NO_2$ and $-Br$) substituted derivatives can serve as chromogenic F^-/CH_3COO^- chemosensors.

1. Introduction

The development of chemosensors for anions has received a significant amount of attention in recent years because anions play an important role in a wide range of biological, environmental, and chemical processes [1–10]. Especially, fluorescent chemosensors that show the shift of emission bands upon binding to anions appear to be particularly attractive due to its simplicity, high sensitivity, and high selectivity [11,12]. For quantitative analyses, ratiometric chemosensors have significant advantages of their dual emission system, which can minimize the measurement errors caused by fluctuations of light scattering as well as reagent concentration [13]. Fluoride, the smallest anion, has unique chemical properties. It is of particular interest to detect and recognize it owing its essential and great potential roles in a broad range of biological, medical, and chemical processes of osteoporosis, fluorination of drinking water supplies, or even in chemical and nuclear warfare agents [14–17]. Different signaling mechanisms have been suggested for F^- chemosensors, such as photoinduced electron transfer (PET) [18], excited state proton transfer (ESPT) [19], intramolecular charge transfer (ICT) [20,21], excimer and exciplex formation [22], and metal–ligand charge transfer (MLCT) [23].

Substances containing thiazole fragment are promising chemosensors for F^-, Cu^{2+}, and Zn^{2+} [24–27]. Recently, a ratiometric fluorescent as well as chromogenic fluoride chemosensor made of 2-(2′-hydroxyphenyl)-4-phenylthiazole (**1**, Scheme 1), has been reported [24]. **1** can undergo the excited state intramolecular proton transfer (ESIPT) to yield excited keto (**II**) form from the original enol (**I**) form and emit strong ESIPT fluorescence. F^- induced color change allows its detection with naked eyes. Interactions of **1** with F^- cause a red-shift in UV–vis absorption and a large Stokes shift in fluorescence emission due to the inhibition of ESIPT induced by the deprotonation of phenolic proton by F^-. To the best of our knowledge, no calculations about both the host–guest interaction and signaling properties have been reported so far.

Herein we report the investigation of both host–guest interaction and signaling properties from theoretical point of view for this system. Further in-deep explanations for the experimental results have been discussed by the investigation of the optical and electronic properties of **1**. To investigate the substituents effects, several derivatives (**2–8**) with electron-donating ($-CH_3$, $-OCH_3$, and $-N(CH_3)_2$) or electron-withdrawing ($-CN$, $-NO_2$, $-COCH_3$ and $-Br$) groups, as shown in Scheme 1, have been designed to provide a demonstration for the rational design of novel fluorescent and chromogenic chemosensors for fluoride anion.

2. Computational methods

All calculations have been performed using Gaussian 09 code [28]. Optimizations have been carried out without symmetry constraints. The geometries of the enol (**I**) and keto (**II**) forms for **1–8** in ground states (S_0) have been optimized by using the hybrid B3LYP functional with 6-31G(d) basis set. Furthermore, complexes consisting of **I** forms of **1–8** and X^- (X = F, Cl, Br, and NO_3), $\mathbf{n}^-$·HF

* Tel.: +86 0476 2205996; fax: +86 0476 2205996.
E-mail address: Ruifajin@163.com.

0022-1139/$ – see front matter © 2011 Elsevier B.V. All rights reserved.
doi:10.1016/j.jfluchem.2011.07.003

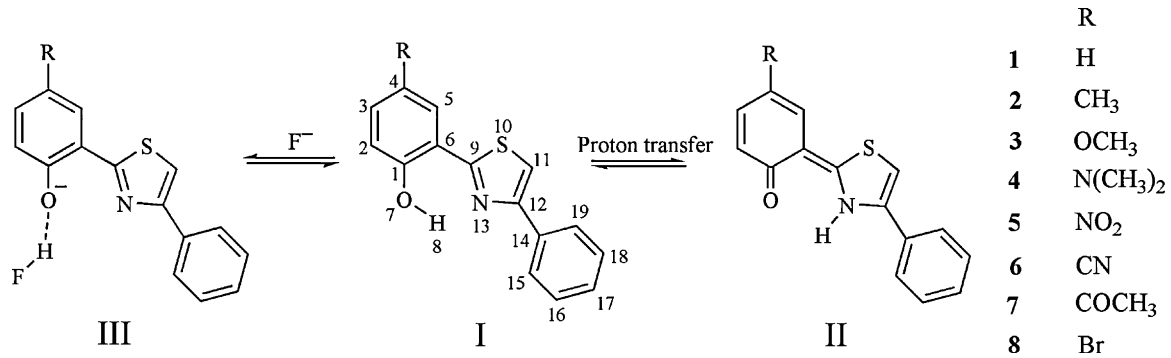

Scheme 1. Geometries of the model compound **1** and its derivatives **2–8** and their deprotonation chemosensing processes for F^-, along with atom numbering.

(**III**) and **n**·X^- (*n* = 1–8, X = Cl, Br, and NO_3), have been optimized at the same theoretical levels as above with the consideration of BSSE correction using the counterpoise method [29]. The first excited singlet state (S_1) structures for **I**, **II**, and **III** (deprotonated complexes **n**$^-$·HF) forms for **1–8** have been optimized at the TD-DFT level using the 6-31G(d) basis set. The harmonic vibrational frequency calculations using the same methods as for the geometry optimizations were used to ascertain the presence of a local minimum. Absorption and fluorescent properties of **I**, **II**, and **III** forms for **1–8** have been predicted using the TD-B3LYP/6-31 + G(d,p) method based on the S_0 and S_1 optimized geometries, respectively. To investigate the influence of solvents on the optical properties for the S_0 and S_1 states of the molecular systems in CH_3CN (dielectric constant: 35.69) solvent, we performed the polarized continuum model (PCM) [30] calculations at the TD-DFT level.

The gas phase acidity of the phenolic proton was computed at 298 K as the enthalpy difference between the anion (ArO^-) and its neutral species (ArOH) [31]:

$$\Delta H_{acidity} = H_{ArO^-} - H_{ArOH}$$

For the calculations in the condensed phase, the acidities were computed in terms of total free salvation energies (ΔG). The pK_a values in solution were obtained by dividing the relative total free energies by 1.37 as a consequence of the following relation:

$$pK_a = \frac{\Delta G}{\ln(10)RT}$$

where *R* is the gas constant and *T* is the absolute temperature. The relative pK_a between **2–8** and **1** is calculating using $\Delta pK_a = \Delta G/1.37$

To gain additional insight into the bonding characteristics of the studied complexes consisting of **1–8** and X^- (X = F, Cl, Br, and NO_3), we have also used the atoms in molecules (AIM) [32,33] theory at the B3LYP/6-31 + G(d,p) level.

3. Results and discussion

3.1. Host–guest interaction

In order to obtain insight into the anion-sensing mechanism, the interactions between hosts and guests have been investigated exploiting the density functional method. The main geometrical parameters and interaction energies with and without BSSE corrections for complexes **1**$^-$·HF and **1**·X^- (X = Cl, Br, and NO_3) are given in Table 1. The Cartesian coordinates of **1** and **1**$^-$·HF are given in Table SI in Supporting Information. According to the suggested geometry cutoffs for D–H···A hydrogen bond definition, i.e., H···A distances <3.0 Å and D–H···A angles >110° [34,35], the interaction between hydroxy H_8 and O_7 for complex **1**$^-$·HF and between Cl, Br, and NO_3 and H_8 in **1**·X^- (X = Cl, Br, and NO_3) can be identified as hydrogen bonds. Comparing the optimized geometries with and without BSSE correction, one may find that the deviation of the hydrogen bond length between hydroxy O and H ($R_{H_8\cdots O_7}$) and the distance between H and F (R_{H_8-F}) for complex **1**$^-$·HF are 0.077 and 0.012 Å, respectively. The deviation of the angles $\theta_{O_7-H_8-F}$ for **1**$^-$·HF is about 7°. Therefore, BSSE correction is necessary for the optimization of this kind of system to some extent. Compared with the H_8–O_7 bond in **I** form of **1** (0.992 Å), obviously, the H_8–O_7 bond is stretched (>0.50 Å elongation) and H^+ moves close to F^- with $R_{H_8\cdots O_7} = 1.598$ Å and $R_{H_8-F} = 0.976$ Å forming **1**$^-$·HF (the R_{H-F} value of HF molecule is 0.988 Å at this level of theory), or more precisely as deprotonated complex **1**$^-$·HF. Namely, the hydroxy moiety can be efficiently deprotonated by F^- and forms covalent type bond H_8–F (see Section 3.2). In the cases of Cl^-, Br^-, and NO_3^-, however, $R_{H_8-O_7}$ values only change slightly (<0.04 Å elongation, see Table 1). Therefore, the host chemosensor substrate prefers to bind with F^- anion and forms the most stable complex **1**$^-$·HF. A few computational studies relating to this type of complex structure can be found in the literature [36,37]. For Cl^-, Br^-, and NO_3^-, the host chemosensor prefers to form the hydrogen-bonded complexes between **1** and Cl^-, Br^-, and NO_3^-, rather than formation of deprotonated complexes. Similar phenomena are also found for **2–8**.

Table 1
The distances of R_{N-H} and $R_{H\cdots X}$ (Å), angles of $\theta_{O-H\cdots X}$ (°), and interaction energies with and without BSSE corrections (kcal/mol) for complexes **1**$^-$·HF and **1**·X^- (X = Cl, Br, and NO_3) at the B3LYP/6-31G(d) level.

Species	Without BSSE				With BSSE			
	$R_{H_8-O_7}$	$R_{H_8\cdots X}$	$\theta_{O_7-H_8\cdots X}$	ΔE	$R_{H_8-O_7}$	$R_{H_8\cdots X}$	$\theta_{O_7-H_8\cdots X}$	ΔE_{BSSE}
1	0.992							
1$^-$·HF	1.521	0.988	165.8	−85.0	1.598	0.976	172.7	−65.3
1·Cl^-	1.026	1.971	160.3	−13.6	1.024	2.004	158.6	−9.7
1·Br^-	1.018	2.137	162.7	−15.8	1.016	2.213	156.1	−7.1
1·NO_3^-	1.020	1.616	158.0	−16.3	1.019	1.647	155.5	−8.1

It is well-known that the electronic reorganization derived from the formation of a hydrogen bond is associated with a charge transfer between the two moieties of the complex [35]. The overall NBO charge transfer has been evaluated by summing up the NBO atomic charges on the two moieties of each hydrogen-bonded complex (the host chemosensor **1** and F^-, Cl^-, Br^-, or NO_3^-). The calculated NBO charge densities are collected in Table SII in Supporting Information. It clearly shows that the negative charge centered on the most electronegative atom, fluorine, is the lowest (−0.674) among F^-, Cl^-, Br^-, and NO_3^-. Moreover, one can see that the sum of the charges on the hydroxyl hydrogen of **1** and F are only about −0.082. The sums are much higher about −0.35 in the case of Cl^-, Br^-, or NO_3^-. Hence, the NBO charge analysis also indicates that the proton is almost completely abstracted by F^- and forms complex $\mathbf{1}^-$·HF.

Furthermore, it is clear that the BSSE-corrected interaction energy (ΔE_{BSSE}) of complex $\mathbf{1}^-$·HF is much more favorable for the distinct selectivity of F^- than other anions. The ΔE_{BSSE} of $\mathbf{1}^-$·HF is more than six times as those of **1**·X^- (X = Cl, Br, and NO_3). Therefore, the sensor can easily detect F^- in the presence of Cl^-, Br^-, and NO_3^-. These calculation results are in good agreement with the reported experimental observations. The intermolecular proton transfer (IPT) between chemosensor substrate **1** and F^- anion occurs when the concentration of F^- anions reaches certain level from the addition of tetrabutylammonium fluoride to the sensor substrate solution, whereas it was not the case for Cl^-, Br^-, and NO_3^- [24].

3.2. Substituent effects

To investigate the effects of different substituents on the acidities of the phenolic protons for substituted derivatives and the ΔE_{BSSE} of the derivatives complexes, a diverse set of 7 substituted derivatives of **1** have been considered. The properties of the different electron donors or acceptors can be nicely summarized in terms of the Hammett sigma para constants (σ_p), one of the most widely used means for the study and interpretation of reactions mechanisms and properties of organic compounds [38,39]. A positive value of σ_p indicates that the substituent group is electron-withdrawing in nature; on the other hand, a negative value implies the electron-donating nature of the substituent. The σ_p values are taken from the compilations of the σ_p by Hansch et al. [40]. On the basis of our previous successful calculation for the effects of substituents on the intramolecular proton transfer and optical properties [41], we exclude the strongest electron-donating group $-N(CH_3)_2$ (σ_p = −0.83) from this system.

Table 2
Gas phase (enthalpies) and CH_3CN (in parentheses) (free energies) acidities of phenolic proton for **1**–**8** at the B3LYP/6-31G(d) level, along with the Hammett sigma para constants (σ_p) of the substituent groups.

n	R	σ_p	Acidities	Relative acidities[a]	Relative pK_a in CH_3CN
1	H	0.00	351.3 (315.0)	0.0 (0.0)	0.0
2	CH_3	−0.17	351.7 (315.6)	0.4 (0.6)	0.44
3	OCH_3	−0.27	353.2 (316.4)	1.9 (1.4)	1.02
4	$N(CH_3)_2$	−0.83	351.3 (316.4)	0.0 (1.4)	1.02
5	NO_2	0.78	332.5 (302.0)	−18.8 (13.0)	−9.5
6	CN	0.66	336.5 (306.1)	−14.8 (−8.9)	−6.5
7	$COCH_3$	0.50	339.9 (307.4)	−11.4 (−7.6)	−5.5
8	Br	0.23	345.0 (311.4)	−6.3 (−3.6)	−2.6

[a] The relative acidities are referred to **1**.

3.2.1. Substituent effects on the ΔE_{BSSE} of substituted derivatives complexes

The interaction energies of the complexes for **1**–**8** are given in Table SIII in Supporting Information. The ΔE_{BSSE} of the deprotonated derivatives complexes $\mathbf{n}^-$·HF (*n* = 1–8) is plotted in Fig. 1a as a function of σ_p (for the σ_p values of the substituent groups, see Table 2). The results displayed in Fig. 1a reveal that the linear correlation (correlation coefficient: R = 0.99 slope: ρ = −16.86) is observed between the ΔE_{BSSE} and σ_p, indicating that the trend in the substituent effects can be qualitatively understood in terms of the electron-donating or -withdrawing character of the substituents. One can also find that the ΔE_{BSSE} decrease with the increasing electron-withdrawing abilities of the substituent (i.e., higher value for σ_p). The ΔE_{BSSE} of electron-withdrawing (-donating) substituted derivatives are smaller (larger) than that of **1**. It suggests that the electron-donating (-withdrawing) groups favor the increase (decrease) for the ΔE_{BSSE} of complexes $\mathbf{n}^-$·HF (*n* = 1–8).

Inspection of Table SIII reveals clearly that the ΔE_{BSSE} values of $\mathbf{n}^-$·HF are more than four times as those of **n**·X^- (*n* = 2–8, X = Cl, Br, and NO_3), respectively. The ΔE_{BSSE} values of $\mathbf{n}^-$·HF for **5**–**8** are more negative 16.0, 12.9, 9.6, and 7.3 kcal/mol than that of $\mathbf{1}^-$·HF, respectively. On the contrary, the corresponding ΔE_{BSSE} values of $\mathbf{n}^-$·HF for **2**–**4** are slightly larger than that of **1** (more positive 0.4, 1.6, and 0.5 kcal/mol), respectively. This indicates that the electron-withdrawing substituents can affect the ΔE_{BSSE} values while electron-donating substituents do not significantly affect the ΔE_{BSSE} values compared with that of **1**. Similar trends are found for complexes **n**·X^- (*n* = 1–8, X = Cl, Br, and NO_3). The complexes **n**·X^- (X = Cl, Br, and NO_3) for **5**–**8** are more negative than those of **1**·X^-

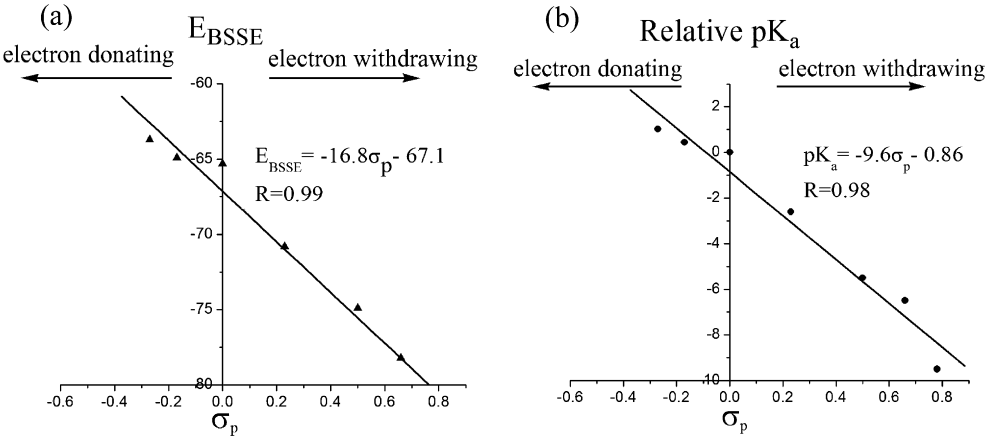

Fig. 1. The ΔE_{BSSE} of the deprotonated derivatives complexes $\mathbf{n}^-$·HF (*n* = 1–8) (a) and the relative pK_a of the derivatives in CH_3CN (b) versus σ_p at the B3LYP/6-31G(d) level.

(X = Cl, Br, and NO_3), while the corresponding ΔE_{BSSE} values of complexes **n**·X^- (X = Cl, Br, and NO_3) for **2–4** are slightly larger than those of **1**·X^- (X = Cl, Br, and NO_3), respectively.

Furthermore, the abilities of hydrogen bond acceptors and donors affect the selectivity of chemosensors. The abilities of hydrogen bond acceptors both CH_3COO^- and $H_2PO_4^-$ are weaker than that of F^- and are stronger than those of Cl^-, Br^-, and NO_3^-. The calculated ΔE_{BSSE} values of **n**·X^- (n = 1–8, X = CH_3COO^- and $H_2PO_4^-$) are given in Table SIV in Supporting Information. As the complexes **n**·X^- (X = Cl, Br, and NO_3), the ΔE_{BSSE} values of **n**·X^- (n = 5–8, X = CH_3COO^- and $H_2PO_4^-$) are more negative than those of complexes **n**·X^- (n = 1–4, X = CH_3COO^- and $H_2PO_4^-$), respectively. Comparing the results shown in Tables SIV with SII, one can find that the ΔE_{BSSE} values of **n**·X^- (n = 1–8, X = CH_3COO^- and $H_2PO_4^-$) are more negative than those of complexes **n**·X^- (n = 1–8, X = Cl, Br, and NO_3) respectively, particularly for CH_3COO^-. The ΔE_{BSSE} values of **n**·CH_3COO^- are more than two times as those of other complexes. Although both CH_3COO^- and $H_2PO_4^-$ are less strong potential hydrogen bond acceptors than that of F^-, they still can form hydrogen bonds with the hydroxyl groups of **5–8**, with large ΔE_{BSSE} values. Therefore, the electron-withdrawing substituents may decrease the selectivity for detecting F^- in the presence of CH_3COO^- and $H_2PO_4^-$, whereas it was not the case for the electron-donating substituents. Thus, one can conclude that the electron-donating substituted derivatives (**1–4**) have much stronger affinity to F^- than to Cl^-, Br^-, NO_3^-, CH_3COO^-, and $H_2PO_4^-$ through intermolecular proton transfer, which leads to the formation of the deprotonated complexes by F^-. However, the selectivity's for detecting F^- of the electron-withdrawing substituted derivatives (**5–8**) may decrease in the presence of CH_3COO^-.

3.2.2. Substituent effects on the acidities of the phenolic protons for the substituted derivatives

The absolute and relative acidities of phenolic proton in gas phase and in CH_3CN solution of **1–8** are collected in Table 2. The relative pK_a of the derivatives in CH_3CN is plotted in Fig. 1b as a function of σ_p. Inspection of Fig. 1b reveals clearly that the relative pK_a linearly decrease with the increase of the electron-withdrawing abilities of substituents (correlation coefficient: R = 0.98, slope: $\rho = -9.6$). The relative pK_a of electron-withdrawing (-donating) substituted derivatives are smaller (larger) than that of **1**. It suggests that the electron-withdrawing (-donating) groups favor the increase (decrease) for the acidities of phenolic protons of the substituted derivatives.

By looking at their molecular structures, **5–8** are characterized a high π-delocalization by introduction of the electron-withdrawing (–CN, $–NO_2$, $–COCH_3$, and –Br) groups. The π-electron can be delocalized over the aromatic ring and the substituents groups. It leads to an increase in the abilities of the hydrogen bond donors (hydroxy groups) for **5–8**, whereas it was not the case for electron-donating substituted derivatives. The trend in gas phase is similar to the CH_3CN solution one. The results displayed in Table 2 reveal that the absolute acidity values for every compound are very much smaller than the corresponding ones in the gas phase. It suggests that the solvent favors the deprotonation process by about 30 kcal/mol. Therefore, the abilities of the hydrogen bond donors (hydroxy groups) of the electron-withdrawing substituted derivatives are stronger than those of the electron-donating substituted derivatives. The abilities of the hydrogen bonds donors (hydroxy groups) of host chemosensors can be tuned by introduction of the electron-withdrawing or electron-donating groups, especially by introduction of electron-withdrawing groups. An increase in the abilities of the hydrogen bond donors (hydroxy groups) for the substituted derivatives favors the deprotonation by F^-. Thus, one can conclude that the host chemosensors have much stronger affinity to F^- than to Cl^-, Br^-, and NO_3^- through intermolecular proton transfer, which leads to the formation of the deprotonated complexes by F^-. The hydrogen bond acceptor F^- is stronger than those of Cl^-, Br^-, and NO_3^-, respectively. On the other hand, the more pronounced the proton transfer reaction, the higher the intensity of the hydrogen bond interaction and the higher the stability of the complex [35,42]. Furthermore, the ΔE_{BSSE}, $R_{H_8-O_7}$, and R_{H_8-X} (X = F, Cl, Br, and NO_3^-) values of complexes also support the distinct selectivity for F^- from Cl^-, Br^-, and NO_3^-.

3.3. AIM analysis

The AIM theory is often applied to study hydrogen bonds. The characteristics of bond critical points (BCPs) are very useful to estimate the strength of hydrogen bonds. To gain a deeper insight into the fundamental nature of OH···X (X = F, Cl, Br, and NO_3) hydrogen bonds, it is crucial to obtain reasonable estimates of their relative energies. In particular, the electron densities, $\rho(r)_{bcp}$, and their Laplacians, $\nabla^2\rho(r)_{bcp}$, evaluated at BCPs are frequently used as indicators of hydrogen bond. More specifically, the potential electron energy density $V(r)_{bcp}$, is often used to gain additional insight on the strength and nature of a given hydrogen bond [43]. The hydrogen bond energy (E_{HB}) in molecules can be estimated within the framework of the AIM analysis using the relationship [44]: $E_{HB} = 0.5\ V(r)_{bcp}$.

Table 3 presents the topological parameters and the hydrogen bond energy E_{HB} of complexes **1**$^-$·HF and **1**·X^- (X = Cl, Br, and NO_3). The corresponding topological parameters of the complexes **n**$^-$·HF and **n**·X^- (n = 2–8, X = Cl, Br, and NO_3) are given in Table SV in Supporting Information. As a general rule, hydrogen bonds are characterized by positive values of $\nabla^2\rho(r)_{bcp}$, low $\rho(r)_{bcp}$ values (<0.1). Covalent bonds (shared interactions) have negative $\nabla^2\rho(r)_{bcp}$ values, high values of $\rho(r)_{bcp}$, whereas the values of $\nabla^2\rho(r)_{bcp}$ become positive when the bonds contain the ionic nature [45]. The results displayed in Table 3 reveal that the $\rho(r)_{bcp}$ and $\nabla^2\rho(r)_{bcp}$ values of $H_8\cdots O_7$ in **1**$^-$·HF are 0.0545 and 0.1404, respectively. It suggests that the interaction between O_7 and H_8 in **1**$^-$·HF is hydrogen bond in nature. The $\rho(r)_{bcp}$ and $\nabla^2\rho(r)_{bcp}$ values of H_6–F in **1**$^-$·HF are 0.2975 and −1.8572. Hence, H_8–F bond in **1**$^-$·HF shows covalent type bond in nature. On the contrary, for complexes **1**·X^- (X = Cl, Br, and NO_3), BCP at H_8–O_7 provides $\nabla^2\rho(r)_{bcp} < 0$ (−1.5616, −1.6494, and −0.1.6272) and high positive values for $\rho(r)_{bcp}$ (0.2972, 0.3022, and 0.2965), which are characteristics of covalent type interactions. For $H_8\cdots X$ bonds in complexes **1**·X^- (X = Cl, Br, and NO_3), the values of $\rho(r)_{bcp}$ and $\nabla^2\rho(r)_{bcp}$ are similar to those of $H_8\cdots O_7$ in **1**$^-$·HF. It indicates that $H_8\cdots X$ bonds in complexes **1**·X^- (X = Cl, Br, and NO_3) show hydrogen bonds in nature. Furthermore, the E_{HB} values of $H_8\cdots O_7$ in **1**$^-$·HF and $R_{H_8\cdots X}$ in **1**·X^- (X = Cl, Br, and NO_3) confirm the expectation. The E_{HB} values of $H_8\cdots O_7$ bonds in **1**$^-$·HF is −13.4 kcal/mol, while the corresponding values of $H_8\cdots X$ bonds for **1**·X^- (X = Cl, Br, and NO_3) are −8.0, −5.3, and −12.3 kcal/mol,

Table 3
The electronic density at BCP $\rho(r)_{bcp}$, the laplacian $\nabla^2\rho(r)_{bcp}$ (all in au), and hydrogen bond energy E_{HB} (in kcal/mol) of complexes **1**$^-$·HF and **1**·X^- (X = Cl, Br, and NO_3) at the B3LYP/6-31 + G(d,p) level.

X	$H_8\cdots O_7$			H_8–X	
	$\rho(r)_{bcp}$	$\nabla^2\rho(r)_{bcp}$	E_{HB}	$\rho(r)_{bcp}$	$\nabla^2\rho(r)_{bcp}$
F	0.0545	0.1404	−13.4	0.2975	−1.8572
X	$H_8\cdots X$			H_8–O_7	
	$\rho(r)_{bcp}$	$\nabla^2\rho(r)_{bcp}$	E_{HB}	$\rho(r)_{bcp}$	$\nabla^2\rho(r)_{bcp}$
Cl	0.0396	0.0648	−8.0	0.2927	−1.5616
Br	0.0306	0.0500	−5.3	0.3022	−1.6496
NO_3	0.0514	0.1348	−12.3	0.2965	−1.6272

respectively. It suggests that the strength of $H_8\cdots O_7$ hydrogen bond in $\mathbf{1}^-\cdot$HF is stronger than those of $H_8\cdots X$ hydrogen bonds in $\mathbf{1}\cdot X^-$ (X = Cl, Br, and NO_3). The above results show qualitative agreement with the results based on their geometries. Similar phenomena are also found for **2**–**8** (see Table SV in Supporting Information).

3.4. Electronic transition

It is useful to examine the frontier molecular orbitals (FMOs) of the compounds under investigation. The origin of the geometric difference introduced by excitation can be explained, at least in qualitative terms, by analyzing the change in the bonding character of the orbitals involved in the electronic transition for each pair of bonded atoms [46]. An electronic excitation results in some electron density redistribution that affects the molecular geometry [46,47]. The qualitative molecular orbital representations of the frontier molecular orbitals (FMOs) for **1** (**I** form) and its deprotonated complex $\mathbf{1}^-\cdot$HF (**III** form) in S_0 are shown in Fig. 2. The major assignments of the lowest electronic transitions for **1** and its deprotonated complex $\mathbf{1}^-\cdot$HF are mainly as HOMO → LUMO, which corresponds to a π–π^* excited singlet state. From Fig. 2, one can see that the HOMO of **1** is spread over the whole conjugated molecule, while its LUMO is mainly localized on phenol and thiazole rings. However, the HOMO of deprotonated complex $\mathbf{1}^-\cdot$HF is mainly localized on phenol and thiazole rings, while its LUMO is spread over the whole conjugated molecule. These results reveal that the F^- has obvious effect on the distribution of FMOs. The distribution patterns of the HOMO and LUMO also provide a remarkable signature for the charge-transfer character of the vertical $S_0 \rightarrow S_1$ transition. Analysis of the FMOs for **1** indicates that the excitation of the electron from the HOMO to LUMO leads the electronic density to flow mainly from the phenol and phenyl rings to thiazole ring. However, the excitation of the electron from the HOMO to LUMO leads the electronic density to flow mainly from the phenol ring to the thiazole and phenyl rings for deprotonated complex $\mathbf{1}^-\cdot$HF. Furthermore, the distribution patterns of FMOs in S_0 state for **1** and $\mathbf{1}^-\cdot$HF suggest a stronger charge-transfer character $\mathbf{1}^-\cdot$HF than that of **1**. The changes in the electronic density for **1** result in an increase in the acidity of the phenolic proton, which favors the deprotonation from **1** to F^- in S_1 state.

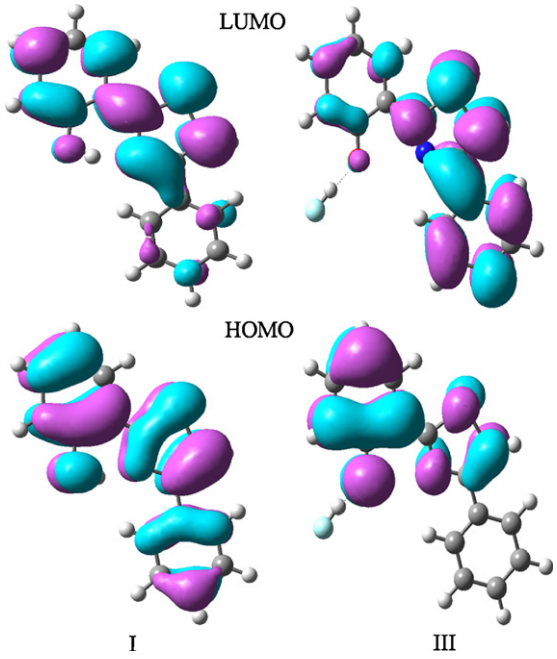

Fig. 2. FMOs of the **I** and **III** forms of chemosensor **1** in S_0 at the B3LYP/6-31G(d) level.

Comparing the geometry **1** with $\mathbf{1}^-\cdot$HF, the bond lengths of C_6–C_9, C_4–C_5, C_2–C_3, and C_1–O_7 are shortened (see Table SI in Supporting Information) after deprotonation, suggesting that the phenol, thiazole, and phenyl rings have strong conjugative effect. As a consequence, the electron can flow easily from phenol moiety to the electron-withdrawing thiazole and phenyl moieties. The photophysical properties of ICT are well known and highly dependent on the electron donor/acceptor strength [48–50]. It is obvious that deprotonation strengthens the electron-donating ability of phenol group. The FMO analyses suggest that the ICT transition in the chemosensor system becomes much easier after deprotonation, resulting in the large bathochromic shift in their absorption and fluorescence spectra.

3.5. Spectral simulation

For the neutral **1**, the absorption corresponds to the excitation of **I** form from S_0 to S_1 state. After the photoexcitation of **I** to the lowest excited singlet state **I***, ultrafast proton transfer will take place and forms keto (**II***) form. Hence, the short-wavelength emission belongs to the emission of **I*** and the long-wavelength emission band characterized by high Stokes shift value is attributed to the emission of **II*** formed by ESIPT. The addition of F^- leads to the intermolecular proton transfer (IPT) between chemosensor **I** and F^- forms deprotonated complex **III** ($\mathbf{1}^-\cdot$HF). This impose a restriction on the occurrence of the intramolecular proton transfer in S_1 state for **I** form and shift the equilibrium from the **II** form towards **III** (see Scheme 1). Hence, the long-wavelength emission of **II*** (506 nm) has strong quenching and new absorption and fluorescence of **III** have been observed when adding enough amounts of fluoride to the sensor's solution. In contrast, the addition of Cl^-, Br^-, and NO_3^- leaves its fluorescence spectra almost unchanged. Therefore, the absorption band can be assigned to **I**, while the emission band belong to **I** and **II** forms before the addition of F^-, respectively. The driving force for the changing of the color and fluorescent intensity is the intermolecular proton transfer. The original color and emissions change upon addition of F^- because of formation **III**. The bathochromic or hypsochromic shifts between the two characteristic absorption of **I** and **III** forms are chosen to calculate the colorimetric fluoride anion chemosensor. The bathochromic or hypsochromic shifts between the two characteristic emissions of **I*** and **III*** forms are chosen to calculate the fluorescent signaling of fluoride anion chemosensor.

Table 4 presents the absorption λ_{abs} and fluorescence λ_{fl} wavelengths, assignments, and the oscillator strength *f* for **1** with and without F^- in CH_3CN at the TD-B3LYP/6-31 + G(d,p) level. The λ_{abs} and λ_{fl} values are all in agreement with experimental results [24], the deviations are within 5 nm, except for the λ_{fl} values of **II** form (the deviation is 44 nm). The λ_{fl} value of **II** form at the same level shows larger deviation from experimental data than those for other forms. The discrepancy may be ascribed to the defect of PCM in the strong polarity for CH_3CN [51,52]. One may conclude that both the predicted λ_{abs} values for **1** and $\mathbf{1}^-\cdot$HF are in agreement with the experimental results (i.e., λ_{abs} = 332 and 400 nm before and after the addition of F^-). The shift between the two characteristic λ_{fl} values for **1** and $\mathbf{1}^-\cdot$HF is 79 nm, which is comparable to the experimental 84 nm. Thus, this result credits to the computational approach, so appropriate electronic transition energies can be predicted at these levels for such kind of chemosensor. The successful simulations indicate that the observed colorimetric and fluorescent signals truly originate from the formation of the deprotonated complex $\mathbf{1}^-\cdot$HF.

Table 5 presents the absorption wavelengths (λ_{abs}), the oscillator strength (*f*), and main assignments (coefficient) of **I**

Table 4
The absorption (λ_{abs}) and fluorescence (λ_{fl}) wavelengths (in nm), the oscillator strength *f*, and assignments (coefficient) for **1** with and without F^- in CH_3CN at the TD-B3LYP/6-31 + G(d,p) level, along with available experimental data.

Conditions	Absorption				Fluorescence			
	λ_{abs}.	*f*	Assignments	Exp[a]	λ_{fl}	*f*	Assignments	Exp[a]
Without F^-	333 (**I**)	0.32	H → L (0.68)	332	369 (**I**)	0.30	H ← L (0.68)	369
					462 (**II**)	0.09	H ← L (0.70)	506
With F^-	397 (**III**)	0.20	H → L (0.70)	400	448 (**III**)	0.05	H ← L (0.70)	453

[a] Experimental results were taken from Ref. [24].

and **III** forms for **1**–**8** in CH_3CN. The λ_{abs} of **I** forms for **2**–**8** are similar to that of **1**, the deviations are within 11 nm, except for **3**. The λ_{abs} of **I** form for **3** has bathochromic shifts compared with that of the parent compound **1**, the deviation is 34 nm. In general, larger oscillator strength corresponds to larger experimental absorption coefficient or stronger fluorescence intensity. The *f* values of **2**–**8** are similar to that of **1**, except the *f* values of **3** and **4** are slightly less than that of **1**. For the **III** forms of the substituted derivatives, it is found that the λ_{abs} values of **III** form for electron-donating substituted derivative (**2**–**4**) are similar to that of the parent compound **1**, except $-N(CH_3)_2$) substituted derivative shows bathochromic shifts (the deviations are within 41 nm). The λ_{abs} value of **III** forms for electron-withdrawing substituted derivatives (**5**–**8**) have hypsochromic shifts compared with that **III** form of **1** (the deviations are within 22 nm), except the λ_{abs} value of **8** is similar to that of **1**. The **III** forms of **5**–**8** show larger *f* values than that of **1**, while the corresponding values of **III** forms for **2**–**4** are similar to that of **1**. It clearly shows that the $-OCH_3$ substitution has more influence on the shifts of λ_{abs} values for the substituted derivative and its **III** form, while the other substitution does not significantly affect the λ_{abs} of the substituted derivatives and their **III** forms. Furthermore, both **I** and **III** forms of electron-withdrawing substituted derivatives (**5**–**8**) show the most intensive spectrum among the substituted derivatives.

In order to well understand the substituent effect on the optical property of chemosensors, we select the parent compound (**1**), electron-donating (**3**), and electron-withdrawing (**6**) substituted derivatives as representatives of the system under investigation. The λ_{abs} and λ_{fl} of their complexes **n**·CH_3COO^- and **n**·$H_2PO_4^-$ (*n* = 1, 3, and 6) are given in Tables SVI and SVII in Supporting Information, respectively. Comparing the results shown in Table SVI with Table 5, one can find that the λ_{abs} values of **n**·$H_2PO_4^-$ (*n* = 1, 3, and 6) are similar to those of **1**, **3**, and **6** respectively, all of the deviations are within 20 nm. It implies that $H_2PO_4^-$ does not significantly affect the absorption spectra of **1**, **3**, and **6**. For **n**·CH_3COO^- (*n* = 1, 3, and 6), the λ_{abs} values of **1**·CH_3COO^- (395 nm) is almost equal to that of **1**$^-$·HF (397 nm). The bathochromic shifts between the two characteristic λ_{abs} values of **1** for CH_3COO^- (i.e., λ_{abs} values before and after the addition of CH_3COO^-) is 62 nm, while the corresponding values for F^- is 64 nm. However, the *f* value of **1**$^-$·HF is larger than that of **1**·CH_3COO^-, indicating that the absorption intensity of **1**·CH_3COO^- is lower than that of **1**$^-$·HF. This is in agreement with experimental results [24]. Same phenomenon is found for **6**·CH_3COO^-. The λ_{abs} value of **6**·CH_3COO^- (369 nm) is similar to that of **6**$^-$·HF (372 nm). This indicates that both F^- and CH_3COO^- showed significant changes for the absorption spectra of **1** and **6** over other anions. However, the λ_{abs} value of **3**·CH_3COO^- is almost equal to that of **3**, the deviation is only 9 nm. Therefore, one can conclude that the CH_3COO^- may affect the selectivity for F^- of electron-withdrawing substituted chemosensors and does not significantly affect the selectivity for F^- of electron-donating substituted chemosensors.

On the basis of the λ_{abs} displayed in Table 5, one can conclude that the $-CH_3$ and $-OCH_3$ substituted derivatives (**2** and **3**) are expected to be chromogenic chemosensors. The bathochromic shifts between the two characteristic λ_{abs} values of **I** and **III** forms (i.e., λ_{abs} values before and after the addition of F^-) for **2**–**8** are 68, 71, 80, 58, 36, 42, and 55 nm, respectively. Therefore, the colorless solutions of **2** and **3** turn yellow and orange yellow in the present F^-, respectively. However, **4**–**8** do not suit to be a chromogenic chemosensor for F^- because the λ_{abs} values for both **I** and **III** forms are in near the UV spectrum. It suggests that the colorless solutions of **4**–**8** have no obvious change for naked eyes upon addition of F^-.

Table 6 presents the fluorescence wavelengths (λ_{fl}) and the oscillator strength (*f*) of **I** and **III** forms for **1**–**8** in CH_3CN. The fluorescence wavelengths (λ_{fl}) and the oscillator strength (*f*) of **II** forms for **1**–**8** in MeCN are given in Table SVIII in Supporting Information. The short-wavelength λ_{fl} values of **I** forms for **1**–**8** show bathochromic shifts, except the corresponding values of **4** and **5** show slightly hypsochromic shift compared with that of **1**,

Table 5
The absorption wavelengths λ_{abs} (in nm), the oscillator strength *f*, and main assignments (coefficient) of **I** and **III** forms for **1**–**8** in CH_3CN at the TD-B3LYP/6-31 + G(d,p) level, along with available experimental data.

n	**I**				**III**			
	λ_{abs}	*f*	Assignment	Exp[a]	λ_{abs}	*f*	Assignment	Exp[a]
1	333	0.32	H → L (0.68)	332	397	0.20	H → L (0.70)	400
2	340	0.30	H → L (0.68)	338	408	0.19	H → L (0.70)	410
			H-1 → L (−0.12)					
3	367	0.20	H → L (0.69)		438	0.19	H → L (0.70)	
4	322	0.15	H → L + 1 (0.54)		402	0.20	H → L (0.70)	
			H-1 → L (0.44)					
5	334	0.29	H → L + 1 (0.69)		392	0.30	H → L (0.66)	
			H → L + 2 (0.10)				H → L + 1 (0.16)	
6	336	0.30	H → L (0.69)		372	0.25	H → L (0.69)	
			H → L + 2 (0.11)					
7	333	0.31	H → L (0.66)		375	0.25	H → L (0.69)	
			H → L + 1 (0.17)					
8	343	0.30	H → L (0.69)	340	398	0.23	H → L (0.70)	410
			H-1 → L (0.11)					

[a] Experimental results were taken from Ref. [24].

Table 6
The fluorescence wavelengths λ_{fl} (nm), the oscillator strength *f*, and main assignments (coefficient) of **I** and **III** forms for **1**–**8** in CH_3CN at the TD-B3LYP/6-31 + G(d,p) level, along with available experimental data.

n	**I**				**III**			
	λ_{fl}	*f*	Assignment	Exp[a]	λ_{fl}	*f*	Assignment	Exp[a]
1	369	0.30	H ← L (0.68)	369	448	0.05	H ← L (0.70)	453
2	388	0.21	H ← L (0.69) H-1 ← L (0.12)	373	474	0.04	H ← L (0.70)	469
3	428	0.16	H ← L (0.70)		522	0.04	H ← L (0.71)	
4	331	0.22	H-1 ← L (0.69) H-1 ← L + 1 (0.11)		598	0.04	H ← L (0.71)	
5	348	0.36	H ← L + 1 (0.69)		391	0.27	H ← L (0.59) H ← L + 1 (0.34)	
6	392	0.30	H ← L (0.70) H ← L + 2 (0.10)		396	0.08	H ← L (0.69)	
7	385	0.32	H ← L (0.69) H ← L + 2 (0.11)		406	0.07	H ← L (0.70)	
8	383	0.27	H ← L (0.69) H-1 ← L (0.12)	378	438	0.06	H ← L (0.70)	457

[a] Experimental results were taken from Ref. [24].

respectively. The long-wavelength λ_{fl} values (**II** forms) of the electron-withdrawing substituted derivatives (**5**–**7**) show strong hypsochromic shifts, while the corresponding values of the electron-donating substituted derivative (**2**–**4**) show strong bathochromic shifts 27–81 nm compared with that of **1**, except the corresponding value of **8** is similar to that of **1**. For the deprotonated complexes **III**, one can find that λ_{fl} values of **III** for the electron-donating substituted derivatives (**2**–**4**) show bathochromic shifts 26, 74, and 150 nm, while the corresponding values of the electron-donating substituted derivatives (**5**–**8**) show hypsochromic shifts 57, 52, 42, and 10 nm compared with that of **1**, respectively. Hence, all substituent groups on the phenol ring can significantly affect the fluorescence spectra of **III** forms for the substituted derivatives. Furthermore, the *f* values of **III** forms for the electron-donating substituted derivative (**2**–**4**) are similar to that of **1**, while the corresponding values of the electron-donating substituted derivatives (**5**–**8**) are larger than that of **1**. Moreover, the *f* value of long-wavelength λ_{fl} for the $-NO_2$ substituted derivative (**5**) is the largest among the derivatives, corresponding to strong fluorescence spectra. Thus, one may conclude that the fluorescence intensity can be increased by introduction of the electron-withdrawing group on the phenol ring moiety of **1**.

Furthermore, as listed in Table SVII, the λ_{fl} values of **1**·CH_3COO^- and **1**·$H_2PO_4^-$ are 488 and 479 nm, respectively. However, their *f* values are smaller than that of **1**$^-$·HF, indicating that the fluorescence intensities of **1**·CH_3COO^- and **1**·$H_2PO_4^-$ are lower than that of **1**$^-$·HF. This is in agreement with experimental results [24]. The λ_{fl} values of **3**·CH_3COO^- and **3**·$H_2PO_4^-$ are 545 and 576 nm, respectively. Their *f* values are smaller than that of **3**$^-$·HF. It suggests that both **3**·CH_3COO^- and **3**·$H_2PO_4^-$ show the fluorescence spectrum as **3**$^-$·HF at about 530 nm and low fluorescence intensities. For **6**·CH_3COO^- and **6**·$H_2PO_4^-$, their λ_{fl} values (404 and 387 nm) are similar to that **6**$^-$·HF (396 nm). The *f* value of **6**·CH_3COO^- is equal to that of **6**$^-$·HF and is larger than that of **6**·$H_2PO_4^-$. This indicates that **6** suit to be a ratiometric fluorescent chemosensors for F^-/CH_3COO^-. Therefore, one can conclude that the electron-withdrawing substituted derivatives may serve as chromogenic F^-/CH_3COO^- chemosensors, whereas the electron-donating substituted derivatives are expected to be the promising candidates for F^- chemosensors only.

The λ_{fl} displayed in Table 6 and the ΔE_{BSSE} values indicate that all the electron-donating substituted derivatives (**2**–**4**) are expected to be promising candidates for ratiometric fluorescent fluoride chemosensors. The bathochromic shifts between the two characteristic λ_{fl} values of **I** and **III** forms (i.e., λ_{fl} values before and after the addition of F^-) for **2**–**4** are 86, 94, and 267, respectively. Therefore, the blue (**2**) and blue-purple (**3** and **4**) original emissions of **2**–**4** may be quenched and new cyanine, green, and yellow emissions appear upon the addition of F^-, respectively. For the electron-withdrawing substituted derivatives (**5**–**8**), the bathochromic shifts between the two characteristic λ_{fl} values of **I** and **III** forms for **5** and **8** are 43 and 55 nm, respectively. This implies that the colorless original emission of **5** and **8** are quenched, along with the appearance of new purple and navy blue emissions upon addition of F^-/CH_3COO^-, respectively. However, **6** and **7** do not suit to be a ratiometric fluorescent fluoride chemosensors because the hypsochromic shift between the two characteristic λ_{fl} values of **I** and **III** forms are only 4 and 21 nm, respectively. This implies that the purple original emissions of both **6** and **7** have no obvious change upon addition of F^-.

We select **5** and **8** as representatives of the chromogenic fluoride chemosensors under investigation and investigate their fluorogenic properties (See detail discussion and Figs. SI and SII in Supporting Information).

4. Conclusions

Our calculated results for both the host–guest interaction and the nature of colorimetric and fluorescent signaling for **1** in the presence of F^- are in good agreement with the reported experimental observations. The host chemosensor **1** has much stronger affinity to F^- than to Cl^-, Br^-, and NO_3^- through intermolecular proton transfer, which leads to the formation of deprotonated complex **1**$^-$·HF by F^-. The AIM theory analysis of the complexes consisting of **1** and X^- (X = F, Cl, Br, and NO_3) confirm that the protons are almost completely abstracted by F^-. The FMO analysis has turned out that the vertical electronic transitions of absorption and emission for **1** and its deprotonated complex **1**$^-$·HF corresponding to the sensing signals are characterized as intramolecular charge transfer (ICT). The shifts of the signals are induced by the increases of donor strength and molecular conjugation when deprotonated by an external F^-. As a consequence, the ICT transition becomes much more efficient when the chemosensor is deprotonated by F^-. The study of substituent effects suggest that the electron-donating $-CH_3$ and $-OCH_3$ substituted derivatives are expected to be promising candidates for ratiometric fluorescent F^- chemosensors as well as chromogenic chemosensors, while electron-donating $-N(CH_3)_2$ substituted derivative can serve as chromogenic F^- chemosensors only. Furthermore, the electron-withdrawing ($-NO_2$ and –Br) substituted derivatives can serve as chromogenic F^-/CH_3COO^- chemosensors.

Acknowledgement

Financial support from the Research Program of Sciences at Universities of Inner Mongolia Autonomous Region (NJzy08148) is gratefully acknowledged.

Appendix A. Supplementary data

Supplementary data associated with this article can be found, in the online version, at doi:10.1016/j.jfluchem.2011.07.003

.

References

[1] A. Bianchi, K. Bowman-James, E. Garcia-Espana, Supramolecular Chemistry of Anions, Wiley-VCH, New York, 1997.
[2] H.W. Rhee, J.C. So, H.Y. Sang, O.J. Yong, H.P. Hun, R.M. Pinto, J.C. Cameselle, F.J. Sandoval, S. Roje, K. Han, D.S. Chung, J. Suh, J.I. Hong, J. Am. Chem. Soc. 131 (2009) 10107–10112.
[3] Y. Qu, J. Hua, H. Tian, Org. Lett. 12 (2010) 3320–3323.
[4] Y. Deng, Y. Chen, D. Cao, Z. Liu, G. Li, Sens. Actuators B: Chem. 149 (2010) 165–169.
[5] M.A. Palacios, R. Nishiyabu, M. Marquez, P. Anzenbacher, J. Am. Chem. Soc. 129 (2007) 7538–7544.
[6] K.R. Dey, B.M. Wong, Md.A. Hossain, Tetrahedron Lett. 51 (2010) 1329–1332.
[7] J.Q. Li, X.Y. Li, J. Phys. Chem. A 111 (2007) 13061–13068.
[8] S. Hagihara, H. Tanaka, S. Matile, J. Am. Chem. Soc. 130 (2008) 5656–5657.
[9] J. Yoon, S.K. Kim, N.J. Singh, K.S. Kim, Chem. Soc. Rev. 35 (2006) 355–360.
[10] P.A. Gale, Acc. Chem. Res. 39 (2006) 465–475.
[11] J.F. Callan, A.P. de Silva, D.C. Magri, Tetrahedron 61 (2005) 8551–8588.
[12] R. Martinez-Manez, F. Sancanon, Chem. Rev. 103 (2003) 4419–4476.
[13] B. Valeur, Molecular Fluorescence, Wiley-VCH, Weinhein, Germany, 2002.
[14] M. Cametti, K. Rissanen, Chem. Commun. 20 (2009) 2809–2829.
[15] K.L. Kirk, Biochemistry of the Halogens and Inorganic Halides, Plenum Press, New York, 1991, 58.
[16] L.V. Avioli, Face, Endocrinol. Metab. Clin. North. Am. 27 (1998) 411–418.
[17] S.W. Zhang, T.M. Swager, J. Am. Chem. Soc. 125 (2003) 3420–3421.
[18] S.K. Kim, J. Yoon, Chem. Commun. 7 (2002) 770–771.
[19] X. Peng, Y. Wu, J. Fan, M. Tian, K. Han, J. Org. Chem. 70 (2005) 10524–10531.
[20] Z. Li, J. Zhang, Chem. Phys. 331 (2006) 159–163.
[21] V. Thiagarajan, P. Ramamurthy, J. Lumin. 126 (2007) 886–892.
[22] S.K. Kim, J.H. Bok, R.A. Bartsch, J.Y. Lee, J.S. Kim, Org. Lett. 7 (2005) 4839–4842.
[23] C.F. Chow, B.K.W. Chiu, M.H.W. Lam, W.Y. Wong, J. Am. Chem. Soc. 125 (2003) 7802–7803.
[24] A. Helal, N.T.T. Thao, H.-S. Kim, J. Incl. Phenom. Macrocycl. Chem. 66 (2010) 87–94.
[25] A. Helal, H.-S. Kim, Tetrahedron Lett. 50 (2009) 5510–5515.
[26] A. Helal, S.H. Lee, S.H. Kim, H.-S. Kim, Tetrahedron Lett. 51 (2010) 3531–3535.
[27] A. Helal, S.H. Kim, H.-S. Kim, Tetrahedron 66 (2010) 9925–9932.
[28] M.J. Frisch, G.W. Trucks, H.B. Schlegel, G.E. Scuseria, M.A. Robb, J.R. Cheeseman, G. Scalmani, V. Barone, B. Mennucci, G.A. Petersson, H. Nakatsuji, M. Caricato, X. Li, H.P. Hratchian, A.F. Izmaylov, J. Bloino, G. Zheng, J.L. Sonnenberg, M. Hada, M. Ehara, K. Toyota, R. Fukuda, J. Hasegawa, M. Ishida, T. Nakajima, Y. Honda, O. Kitao, H. Nakai, T. Vreven, J.A. Montgomery Jr., J.E. Peralta, F. Ogliaro, M. Bearpark, J.J. Heyd, E. Brothers, K.N. Kudin, V.N. Staroverov, R. Kobayashi, J. Normand, K. Raghavachari, A. Rendell, J.C. Burant, S.S. Iyengar, J. Tomasi, M. Cossi, N. Rega, J.M. Millam, M. Klene, J.E. Knox, J.B. Cross, V. Bakken, C. Adamo, J. Jaramillo, R. Gomperts, R.E. Stratmann, O. Yazyev, A.J. Austin, R. Cammi, C. Pomelli, J.W. Ochterski, R.L. Martin, K. Morokuma, V.G. Zakrzewski, G.A. Voth, P. Salvador, J.J. Dannenberg, S. Dapprich, A.D. Daniels, O. Farkas, J.B. Foresman, J.V. Ortiz, J. Cioslowski, D.J. Fox, Gaussian 09, Gaussian, Inc., Wallingford, CT, 2009.
[29] S. Simon, M. Duran, J.J. Dannenberg, J. Chem. Phys. 105 (1996) 11024–11031.
[30] J.P. Cornard, C. Lapouge, J. Phys. Chem. A 110 (2006) 7159–7166.
[31] M. Leopoldini, N. Russo, S. Chiodo, M. Toscano, J. Agric. Food Chem. 54 (2006) 3078–3085.
[32] R.F.W. Bader, J. Phys. Chem. A 102 (1998) 7314–7323.
[33] AIM2000 designed by Friedrich Biegler-König, University of Applied Sciences, Bielefeld, Germany, 2000
[34] T. Steiner, G.R. Desiraju, Chem. Commun. (1998) 891–892.
[35] T. Steiner, Angew. Chem. Int. Ed. 41 (2002) 48–76.
[36] G.-Y. Li, G.-J. Zhao, Y.-H. Liu, K.-L. Han, G.-Z. He, J. Comput. Chem. 31 (2010) 1759–1765.
[37] R. Jin, J. Zhang, Theor. Chem. Acc. 124 (2009) 225–234.
[38] S.E. Wheeler, K.N. Houk, J. Am. Chem. Soc. 130 (2008) 10854–10855.
[39] G. Fayet, L. Joubert, P. Rotureau, C. Adamo, J. Phys. Chem. A 112 (2008) 4054–4059.
[40] C. Hansch, A. Leo, R.W. Taft, Chem. Rev. 91 (1991) 165–195.
[41] R. Jin, J. Zhang, Theor. Chem. Acc. 124 (2009) 331–338.
[42] V. Amendola, D. Esteban-Gómez, L. Fabbrizzi, M. Licchelli, Acc. Chem. Res. 39 (2006) 343–353.
[43] Y.A. Abramov, Acta Crystallogr. A 53 (1997) 264–272.
[44] E. Espinosa, E. Molins, C. Lecomte, Chem. Phys. Lett. 285 (1998) 170–173.
[45] W. Nakanishi, S. Hayashi, K. Narahara, J. Phys. Chem. A 112 (2008) 13593–13599.
[46] M. Forés, M. Duran, M. Solà, L. Adamowicz, J. Phys. Chem. A 103 (1999) 4413–4420.
[47] A. Helal, M.H.O. Rashid, C.-H. Choi, H.-S. Kim, Tetrahedron 67 (2011) 2794–2802.
[48] B. Liu, H. Tian, J. Mater. Chem. 15 (2005) 2681–2686.
[49] Z. Wen, Y. Jiang, Tetrahedron 60 (2004) 11109–11115.
[50] W. Huang, X. Zhang, L. Ma, C. Wang, Y. Jiang, Chem. Phys. Lett. 352 (2002) 401–407.
[51] C.J. Cramer, D.G. Truhlar, Acc. Chem. Res. 42 (2009) 493–497.
[52] S. Meng, J. Ma, J. Phys. Chem. B 112 (2008) 4313–4322.